19th Australasian Fluid Mechanics Conference
Melbourne, Australia
8-11 December 2014

Performance Considerations for Expansion Tube Operation with a Shock-Heated Secondary Driver

D. E. Gildfind[1], C. M. James[1], and R.G. Morgan[1]

[1]Centre for Hypersonics, School of Mechanical and Mining Engineering,
The University of Queensland, Brisbane, Queensland, 4071, Australia

Abstract

This paper reports on a study examining operation of a shock-heated secondary driver across the entire operating envelope of a free-piston driven expansion tube. It is found that the secondary driver operating characteristics depend significantly on the specific characteristics of the flow condition. Key trends and characteristics are identified, and theoretical concepts are validated by numerical analysis and experiment.

Introduction

The secondary driver was first proposed by Henshall [1] and evaluated experimentally by Stalker and Plumb [2]. It is a modification normally applied to expansion tubes [3, 4], which involves placing a volume of helium between the primary diaphragm and test gas, and is typically used either to increase shock strength through the test gas [3, 4], or to prevent transmission of primary driver disturbances to the test gas [3, 5]. The theoretical principles of secondary driver operation are well established [3, 4], however its effective implementation is non-trivial for two reasons: firstly, the device increases the already large number of facility variables which must each be configured to achieve the desired test condition; secondly, for certain parts of the facility operating envelope, it can introduce complex secondary wave processes [6] which must be accounted for in order to make accurate predictions of the test flow properties.

This paper reports on a study of The University of Queensland's X2 expansion tube operating with a secondary driver. In order to make some conclusions about the wider implications of using this device, it was considered instructive to examine its performance across the entire practical operating envelope of X2, for one of X2's high performance free-piston driver conditions. The study is wide ranging, and has analytical, numerical, and experimental aspects. It is beyond the scope of this paper to document this process in detail, therefore the current paper will present some of the most relevant findings; further detail and justification will be provided in a future extended article.

X2 Facility Operating Envelope with Free-Piston Driver

Figure 1a shows an idealised *x-t* diagram of the flow processes which occur in a basic expansion tube. In Figures 1b and c an additional volume of helium gas is located between the primary diaphragm and the test gas. Depending on the initial ratio of fill pressures between the secondary driver gas (Region *sd*1) and the test gas (Region 1), either an unsteady expansion (Figure 1b) or reflected shock wave (Figure 1c) will process the already shock-processed Region *sd*2 gas after the secondary diaphragm ruptures. The secondary driver is said to be 'over-tailored' when the sound speed of the shock-processed secondary driver gas, a_{sd2}, is higher than that of the expanded driver gas, a_{sd3} (i.e. $a_{sd2} > a_{sd3}$). In Figure 1b, over-tailoring can result in the secondary driver generating a stronger shock through the test gas than the primary driver would be able to by itself; this performance increasing potential was the motivation for initial work with these devices, and has previously been analysed and confirmed experimentally [1, 2, 3, 4].

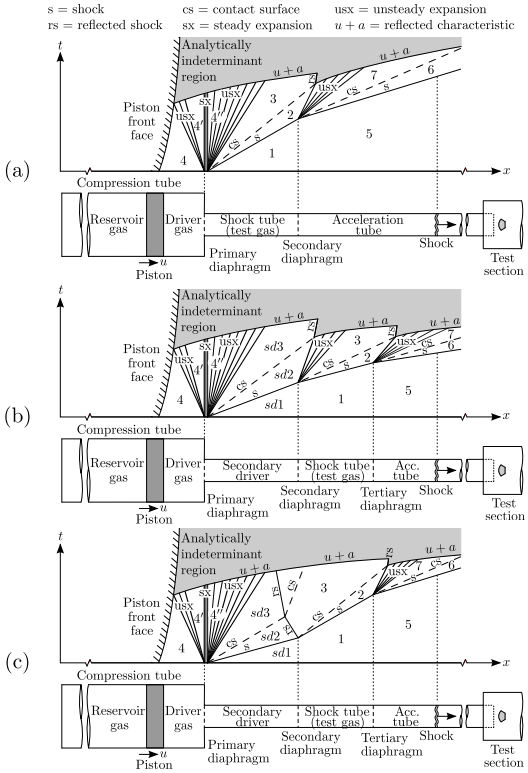

Figure 1. Idealised *x-t* diagram for (a) basic expansion tube; (b) expansion tube with secondary driver and unsteady expansion at secondary diaphragm; (c) expansion tube with secondary driver and reflected shock at secondary diaphragm.

Trimpi's expansion tube analytical framework [8], modified to include an optional secondary driver, was used to calculate X2 flow properties through the various regions shown in Figure 1a–c. The analysis was restricted to using air as the test gas (Regions 1, 2, 5–7), and one of X2's recently developed high performance driver conditions, 'x2-lwp-2.0mm-100He-0' (refer Table 1). Noting that real gas effects become important for air at the flight conditions frequently produced in these facilities, equilibrium properties were calculated using CEA [9] for all air calculations. Helium flow processes were modeled using ideal gas assumptions, which provide good accuracy across the range of temperatures and pressures considered.

Driver condition I.D.	Driver gas composition -	Orifice plate Ø mm	Diaphragm thickness mm	Rupture pressure MPa	Reservoir fill pressure MPa	Driver fill pressure kPa
x2-lwp-2.0mm-100He-0	100% He	65	2.0	27.9	6.85	92.8

Table 1. X2 10.5kg piston tuned driver condition, with effective p and T of 27.4 MPa and 2,903 K respectively [10].

Inspecting Regions 1, 2, and 5–7 in Figure 1(a–c), shock-processing compressively heats the Region 1 test gas, and accelerates it towards the downstream diaphragm separating the test and accelerator gases. When this final diaphragm is ruptured, the Region 2 gas undergoes an unsteady expansion which

is bounded by the initial fill pressure in the acceleration tube, p_5. Ignoring processes upstream of the shock tube for now, and making ideal gas assumptions, it follows that any given test flow condition (i.e. Region 7) will be defined by a single pair of shock speeds through the shock and acceleration tubes, and the ratio of fill pressures p_5/p_1; the static pressure of the final test flow will then depend on the initial shock tube fill pressure, p_1. The fundamental purpose of the driver is therefore to generate a shock of the required strength, through a test gas at the required p_1. If an appropriate p_5 is set, then the test gas will expand to the required condition. These general trends are qualitatively observed even when real gas effects become important.

Based on the above, secondary driver performance was assessed by examining the shock speed through the shock tube. An iterative scheme similar to that detailed in [6] and [7] was developed to calculate test gas shock speeds, for initial air fill pressures ranging from $p_1 = 10^2$ to 10^6 Pa. Referring to Figure 2a, the 'red' surface plot shows the computed shock speed when there is no secondary driver; i.e. the case shown earlier in Figure 1a. The 'grey' surface plot in Figure 2a shows the computed shock speed for secondary driver fill pressures from $p_{sd1} = 10^2$ to 10^6 Pa helium. The grey surface varies with both p_1 and p_{sd1}, showing the dependency of shock speed on both fill pressures; the red plot obviously must be invariant with p_{sd1} since it considers the basic expansion tube without secondary driver.

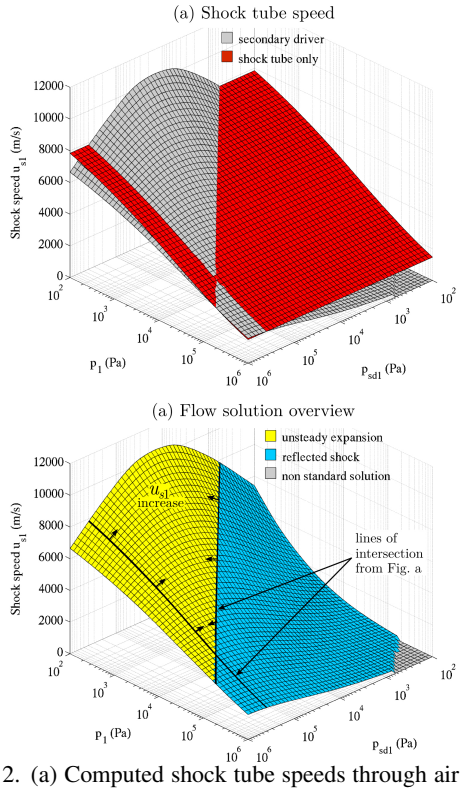

Figure 2. (a) Computed shock tube speeds through air test gas (with and without secondary driver), and (b) solution overview, for X2 driver condition x2-lwp-2.0mm-100He-0 (Table 1).

Figure 2b delineates the operating region where a secondary driver theoretically imparts a performance increase. The 'yellow' region of the surface plot indicates conditions where the secondary driver gas undergoes an unsteady expansion into the test gas (the case shown in Figure 1b). The line running parallel to the p_1 axis, i.e. $p_{sd1} \approx$400 kPa, represents the tailored condition where the sound speed of the expanded primary driver gas, a_{sd3}, is equal to the sound speed of the shock-processed secondary driver gas, a_{sd2} (this is later shown explicity in Figure 5). At even lower secondary driver fill pressures, i.e. p_{sd1} <400 kPa, the condition $a_{sd2} > a_{sd3}$ arises, and the secondary driver is said to be 'over-tailored' with respect to the primary driver gas. This is the fundamental operating regime which allows the secondary driver gas to achieve a stronger shock than the primary driver gas alone [3, 4], and corresponds to a performance increase relative to the basic expansion tube.

However, a diagonal line is also observed in Figure 2b; this marks the boundary of the blue region, which is the region of operation where a reflected shock forms upon rupture of the secondary diaphragm (i.e. the case shown in Figure 1c), and the shock tube shock speed is seen to reduce compared to the basic expansion tube. It was an explicitly stated assumption of earlier studies [4] that the secondary gas must unsteadily *expand* into the test gas in order to utilise its higher sound speed to drive a stronger shock. Nevertheless, observing Figure 2b, it becomes evident that for an air test gas, even though the secondary driver is over-tailored ($a_{sd2} > a_{sd3}$) over most of the sensible facility operating envelope, the requirement that the shock-processed secondary driver gas (region $sd2$) must undergo an unsteady expansion into the test gas - to achieve a performance increase compared to a basic expansion tube - becomes very restrictive.

Whether or not a reflected shock arises at the secondary diaphragm depends both on the ratio of initial fill pressures in the secondary driver and shock tubes (p_{sd1} and p_1 respectively), and on the strength of the resulting shock in the shock tube. For $p_1 << p_{sd1}$, an unsteady expansion will occur; if p_1 is increased, eventually a point will be reached where the unsteady expansion has zero strength; if p_1 is further increased, a reflected shock wave will form. The weakest reflected shock will be a Mach wave, and will produce negligible pressure rise, and negligible deceleration, of the Region $sd2$ flow; for this case $u_{sd2} = u_3$, and $p_{sd2} = p_3$. Although the proof is not provided here, if ideal gas assumptions are made, the fill pressure ratio associated with this condition, $p_{sd1,r}/p_1$, can be solved as a function of test gas shock strength, expressed in terms of p_2/p_1.

Referring to Figure 3, there are two solutions for the reflected Mach wave case. The curve denoted 'Solution 1' is the only physical solution. It can be seen that except for weak shocks, the ratio $p_{sd1,r}/p_1 \approx 6$ indicates the pressure ratio *below which* a reflected shock will form in the secondary driver gas. For $p_{sd1}/p_1 > 6$, the secondary driver gas is sufficiently dense that it will undergo an unsteady expansion into the test gas for all test gas shock speeds. For an air test gas, in practise this effectively limits the use of a secondary driver as a performance increasing device to superorbital conditions only. This limitation will be less restrictive for lighter test gases.

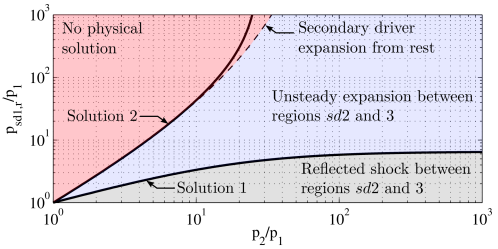

Figure 3. Effect of secondary driver/test gas fill pressure ratio, p_{sd1}/p_1, post-diaphragm rupture flow processes.

Another solution exists for the reflected Mach wave case: 'Solution 2' in Figure 3. This curve is an artifact of the analytical model and therefore non-physical, however it is interesting to note that at low values of p_2/p_1, this curve is aligned with the dashed curve shown in the plot; this dashed curve indicates the strength of shock which the secondary driver will drive through the test gas simply by virtue of its high initial fill pressure; i.e. with no initial velocity, and independent of the upstream driver.

Representative Flow Conditions

The physical implications of the Figure 2 results can be better understood by examining some representative flow conditions:

- High enthalpy flight: representative Mars and Far Solar system return reentry trajectories are shown in Figure 4. These are the hypervelocity, low density, air, flight conditions which a vehicle returning to Earth's atmosphere would undergo. These can only be produced by an expansion tube, and at the upper limits they often depend on the performance increase provided by the secondary driver.
- Low enthalpy flight: scramjet access-to-space flight conditions are shown in Table 2. Expansion tubes become necessary to simulate scramjet flight between Mach 10 and 14, where total pressures soon exceed the capabilities of other facilities which must stagnate their test gas.

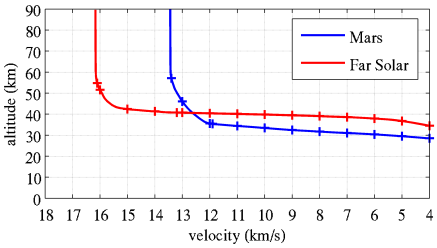

Figure 4. Mars and Far Solar Return Reentry Trajectories [11].

Mach [-]	Altitude [m]	T [K]	V [m/s]	h $MJ/(kgK)$	p [kPa]	p_0 [MPa]
10	29,108	226	3,011	4.76	1.368	128
12	31,552	228	3,633	6.52	0.950	457
14	33,649	233	4,282	9.10	0.698	1,469

Table 2. 95.8kPa scramjet flow conditions.

Flow Condition Mapping

It is recalled that the primary performance challenge for simulating an expansion tube flow condition is achieving the required shock speed through the test gas, for a given p_5. p_5 will vary depending on the model scale and other considerations. An equilibrium gas expansion tube analysis was used to calculate the theoretically required test gas shock speeds to achieve each of the flow conditions detailed in Figure 4 and Table 2. These conditions are mapped onto the facility performance envelope in Figure 5. Two key observations can be made: firstly, the results indicate that each target test condition can be achieved across a range of static pressures; there is a theoretical capacity to control the test flow static pressure even though the primary driver configuration is fixed. Secondly, the majority of scramjet conditions are only achieved in a region of the facility operating envelope where the secondary driver *reduces* net performance.

Results and Analysis

High Enthalpy Example: 13 km/s Mars Return

Figure 6 shows the calculated facility configuration parameters, required shock speeds, and test flow static pressure, for the 13 km/s Mars Return case. It is impractical to achieve true flight Mach number ($M_\infty >> 30$) at these conditions in an expansion tube; instead flight enthalpy is matched, and based on the Mach number independence principle, a higher freestream temperature is selected, producing a freestream $M_7 = M_\infty = 10$. p_7 is compared to both the flight equivalent true static pressure, $p_{m10,f.e.}$, and the static pressure for operation without a secondary driver, $p_{7,no\ sec}$. It can be seen that the secondary driver can significantly outperform the basic expansion tube. Furthermore, it can also act as a test flow static pressure control, which is otherwise only achieved through the more difficult route of

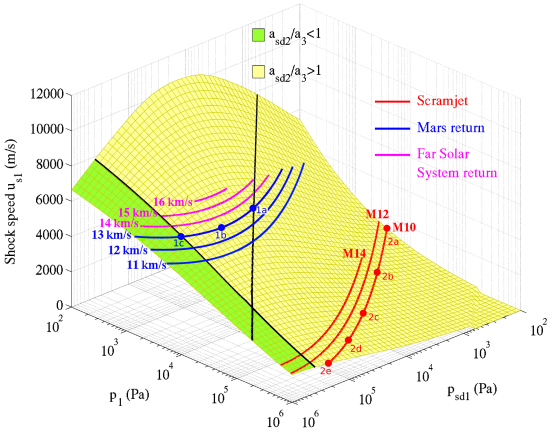

Figure 5. Flow conditions mapped onto performance envelope.

modifying the primary driver itself. Figure 7 shows experimental confirmation of these results in X2. Experimentally measured shock speeds are compared to target values from Figure 6. Secondary driver and test gas shock speeds are closely matched, confirming the analytical results, and demonstrating that the static pressure control mechanism is valid (note: the static pressure in the shock tube is different for each of these experimental results, even though the shock speeds are approximately equal). There is some scatter and uncertainty in the acceleration tube shock speeds; this was due to two reasons: firstly, the pressure sensors in this tube were insufficiently sensitive to precisely identify shock arrival at the transducer; secondly, low fill pressures could not be reliably achieved, or held, at the time of the experiments.

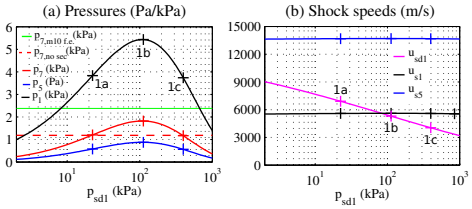

Figure 6. Facility configuration for 13 km/s Mars return.

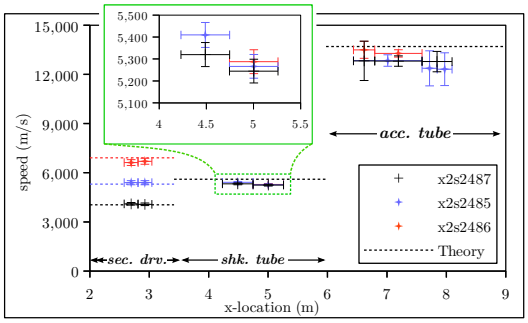

Figure 7. Shock speeds for 13 km/s Mars Return flight equivalent conditions. Vertical error bars represent uncertainty in shock speed measurement; horizontal bars indicate span between transducer pairs used for each time of flight calculation.

Low Enthalpy Example: Mach 10 Scramjet Flight

While a theoretical analysis yields the scramjet conditions 2a–2e in Figure 5, recent experience with these conditions [6, 7] has shown that these calculations become invalid for facility configurations when there is a strong reflected shock through the secondary driver gas. When the secondary diaphragm ruptures in Figure 1c, the shock-processed slug of helium (Region *sd*2) has a short length but high sound speed, and is rapidly processed by the reflected shock wave. This wave then reflects off the $sd2/sd3$ interface, and returns as a strong compression

wave. The timescales for this phenomena are very short compared to other flow processes; for most practical conditions, the secondary driver would need to be an order of magnitude longer than the shock tube to sufficiently delay arrival of this wave. These wave processes have been described in [6], and numerical and experimental results from this study have repeatedly confirmed this. In practise, at low enthalpy conditions with a dense test gas, the secondary driver behaviour is no longer correctly described by traditional theoretical models. The helium has negligible effect on the magnitude of test flow properties, and acts as a passive slug between the primary driver and test gases. These assertions will be thoroughly defended in a future publication on this study, however the effect is shown in Figure 8. Here, the 1-D CFD code L1d [12] has been used to calculate shock speeds along the length of X2. The black curve shows the shock speeds for a Mach 10 scramjet condition without a secondary driver; coloured curves show shock speeds when secondary drivers of differing fill pressures are introduced between the primary diaphragm ($x = 0$) and $x = 3.4$ m. While shock speed obviously varies through the secondary driver, all curves are seen to collapse to the same speeds further downstream.

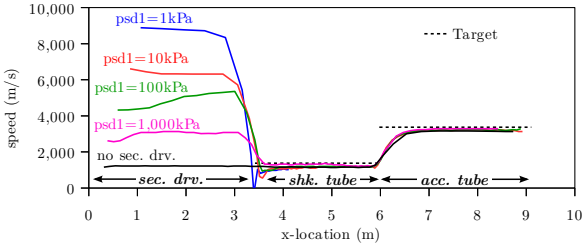

Figure 8. Shock speeds Mach 10 arbitrary secondary driver.

Morgan [3, 4] suggested the use of a secondary driver to act as an 'acoustic buffer' for these types of scramjet conditions, because it had earlier been shown that over-tailored operation can prevent the transmission of driver disturbances from the expanded primary driver gas to the test gas [5]. Figure 9 demonstrates this 'acoustic buffer' using L1d simulations of X2, incorporating full piston dynamics, for the same Mach 10 condition in Figure 8. Figure 9a shows sound speed mapped over an *x-t* diagram for the basic expansion tube; Figure 9a shows the same result with a helium secondary driver initially at 150 kPa. It can be seen that without a secondary driver, the ratio $a_2/a_3 << 1$, and driver noise would be expected to transmit to the test gas [5]; Figure 9b however shows that the inclusion of a secondary driver strongly over-tailors the interface to the primary driver gas, thereby meeting the acoustic buffer requirement.

While this arrangement would theoretically shield the downstream gas from primary driver disturbances, the air (Region 2) is still under-tailored with respect to Region (2*d*3); disturbances arising in the secondary driver gas due to diaphragm rupture, or its passage down the tube, could theoretically be transmitted to the test gas this way. In the absence of competing requirements, it is proposed here that the ideal secondary driver fill pressure is that which exactly matches the test flow fill pressure (assuming this will achieve an overtailored condition, which it often will for high Mach number conditions), since this will require the thinnest diaphragm; such a diaphragm would have the minimum influence on the flow, and introduce minimum noise at the interface when the shock ruptures it.

Conclusion

This paper has provided an overview of results from a study of the use of a secondary driver with an expansion tube. Its performance across the entire operating envelope for the X2 facility has been assessed, and it has been shown that its operating characteristics can vary significantly. At high enthalpies the

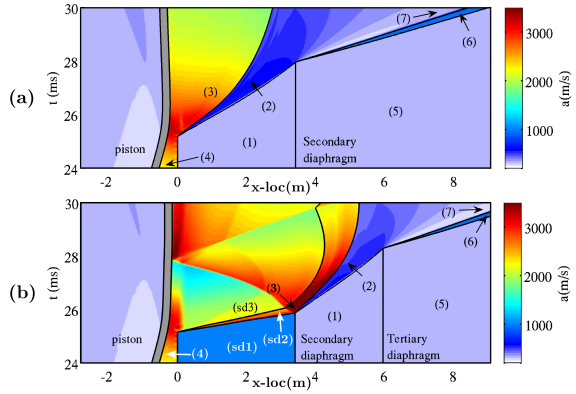

Figure 9. Computed sound speed for Mach 10 scramjet condition (a) without and (b) with 150 kPa helium seconday driver.

secondary driver behaviour largely follows traditional theoretical analyses. However, even in over-tailored operation, when the test gas is initially denser than the secondary driver gas, a reflected shock will form at the $sd3/2$ interface, and lead to an overall performance reduction. This negates the use of the secondary driver for scramjet flow conditions in terms of pure performance, however it theoretically retains its ability to provide an acoustic buffer at these lower enthalpy conditions [4]. Future publications from this study will examine these issues in more detail, and provide more rigorous justification for the ideas proposed in this paper.

References

[1] Henshall, B. (1956): The Use of Multiple Diaphragms in Shock Tubes., *A.R.C. Technical Report C.P. No. 291*.

[2] Stalker, R. and Plumb, D. (1968): Diaphragm-type Shock Tube for High Shock Speeds, *Nature*, **218**:5143, pp. 789-790.

[3] Morgan, R. and Stalker, R. (1991): Double Diaphragm Driven Free Piston Expansion Tube. *18th International Symposium on Shock Waves*, Jul 21-26, Sendai, Japan.

[4] Morgan, R.G. (2001): Chapter: 4.3 Free-Piston Driven Expansion Tubes. In: *Handbook of Shock Waves*, Vol. 1, Ben-Dor, G., Igra, O., and Elperin, T. (Eds.), pp. 603-622.

[5] Paull, A. and Stalker, R. (1992): Test flow disturbances in an expansion tube, *J. Fluid Mech.*, **245**, pp. 493-521.

[6] Gildfind, D.E., Morgan, R.G., McGilvray, M., Jacobs, P.A. (2014): Production of High Mach Number Scramjet Flow Conditions in an Expansion Tube. *AIAA Journal*, **52**:1, pp. 162–177.

[7] Gildfind, D. (2012), *Development of High Total Pressure Scramjet Flow Conditions using the X2 Expansion Tube*, Ph.D. thesis, School of Mechanical and Mining Engineering, The University of Queensland, Brisbane.

[8] Trimpi, R.L. (1962): A preliminary theoretical study of the expansion tube, a new device for producing high-enthalpy short-duration hypersonic gas flows. *NASA Report R-133*.

[9] Gordon, S., McBride, B.J. (994): Computer program for calculation of complex chemical equilibrium compositions and applications. *NASA Technical Report 1311*.

[10] Gildfind, D.E., James, C.M., Morgan, R.G. (2014): Free-Piston Driver Performance Characterisation Using Experimental Shock Speeds Through Helium. *Under review*.

[11] Office of the Chief Engineer (2010): Evaluation of the NASA Arc Jet Capabilities to Support Mission Requirements, NASA/SP-2010-577, May.

[12] Jacobs, P.A. (1994): Quasi-one-dimensional modelling of a free-piston shock tunnel. *AIAA Journal*, **32**(1), pp. 137–145.